ARTICLE

Superparamagnetic-blocked state transition under alternating magnetic fields: towards determining the magnetic anisotropy in magnetic suspensions

Received 00th January 20xx,
Accepted 00th January 20xx

DOI: 10.1039/x0xx00000x

David Cabrera[1,2], Takashi Yoshida[3], Teresa Rincón-Domínguez[1], J.L. F. Cuñado[1,4], Gorka Salas[1,5], Alberto Bollero[1], María del Puerto Morales[6], Julio Camarero[1,4] and Francisco J. Teran*[1,5]

The potential of magnetic nanoparticles for acting as efficient catalysts, imaging tracers or heating mediators under alternating magnetic fields grounds on their superparamagnetic behaviour. In spite of the relevance of this magnetic phenomenon, the identification of specific fingerprints to unequivocally assign superparamagnetic behaviour in nanomaterials is still lacking. Here, we report on novel experimental and theoretical evidences related to superparamagnetism observed in magnetic iron oxide nanoparticle suspensions at room temperature. AC magnetization measurements in a broad field frequency range from mHz to kHz and field intensities up to 40 kA/m unambiguously demonstrate the transition from superparamagnetic to blocked states at room temperature. Our experimental observations are supported by a theoretical model based on a stochastic Landau-Liftshitz-Gilbert equation. In addition, an empirical expression is proposed to determine the effective magnetic anisotropy from the field frequency value beyond which AC magnetization shows hysteretic behaviour. Our results significantly improve the understanding and the description of superparamagnetism of iron oxide nanoparticles, paving the way towards a more efficient exploitation of their unique magnetic properties.

Introduction

Recent progress on material science has allowed to tune the magnetic behaviour of nanomaterials by controlling their size, shape, chemical composition and/or crystallinity.[1-5] Indeed, the bespoken design and synthesis of magnetic nanoparticles has led to the observation and understanding of customised magnetic phenomena.[6] This is the case of superparamagnetism, a magnetic behaviour related to nanoscale-size materials with ferro- or ferrimagnetic order. [7-9.] The latest lead to an spontaneous magnetization related to the net alignment of atomic magnetic spins at temperatures lower than Curie temperature (T_C).[10] Below T_C , single magnetic monodomain structure emerges as a single macroscopic spin defining the nanoparticle magnetic moment (m_{NP}), which depends on nanoparticle material composition, crystallinity and size. Interestingly, thermal fluctuations between preferential magnetic states induce a spontaneous, and fully coherent m_{NP} reversal between energy minima by overcoming a magnetic anisotropy energy barrier ($\Delta E=KV$, where K is the magnetic anisotropy and V the nanoparticle volume)[6,11, 12] In short, superparagnetism is the rupture of directional order of nanoparticle magnetic moments imposed by the magnetic anisotropy. The observation of blocked (BS) or unblocked (SPM) magnetic states depends on the ratio between thermal (k_BT, k_B the Boltzmann constant) and anisotropy energies. The first description of m_{NP} reorientation dynamics -in absence of alternating magnetic fields (AMF)- was proposed by Louis Néel as an Arrhenius equation: [13-15]

$$\tau_N=\frac{1}{2}\sqrt{\frac{\pi}{\sigma}}\tau_{N0}\exp(\sigma) \qquad (1)$$

where $\tau_{N0}=10^{-9}$ s, and $\sigma=KV/k_BT$. Traditionally, the identification of superparamagnetic behaviour grounds on probing the transitions between BS to SPM states at temperatures, higher/ lower than blocking temperature (T_B). But due to temporal and temperature components ruling the m_{NP} orientation, there is not a well-defined transition between BS and SPM states. Contrary to transitions between ferro-/ferrimagnetic and paramagnetic states whose T_C is well established, T_B tightly depends on external magnetic field intensity (H_{AMF}) and frequency (f_{AMF}) employed for magnetization

1 *iMdea Nanociencia, Campus Universitaria de Cantoblanco, 28049 Madrid. Spain.*
2 School of Pharmacy and Bioengineering, Keele University, Guy Hilton Research Centre, Thurnburrow Drive, ST4 7QB, Stoke on Trent, UK.
3 Dpt. of Electrical Engineering, Kyushu University, Fukuoka 819-0385, Japan.
4 Departamento de Física de la Materia Condensada and Instituto 'Nicolás Cabrera', Universidad Autónoma de Madrid, 28049 Madrid, Spain.
5 Nanobiotecnología (iMdea Nanociencia), Unidad Asociada al Centro Nacional de Biotecnología (CSIC), 28049 Madrid, Spain
6 Instituto de Ciencia de Materiales de Madrid-CSIC, Cantoblanco, 28049 Madrid, Spain
E-mail :francisco.teran@imdea.org
Electronic Supplementary Information (ESI) available. See DOI: 10.1039/x0xx00000x

measurements. This is because magnetisation (M) of a nanoparticles ensemble strongly relies on temperature (*T*) and dynamical AMF conditions i.e. H_{AMF} and f_{AMF}. While H_{AMF} defines magnetization polarization, f_{AMF} defines the measurement time (τ_M=1/2πf_{AMF}) related to the AMF sweeping rate during magnetisation measurements. If H_{AMF} is much lower than the coercive field of the nanoparticle ensemble (H_C), *M* will linearly follow H_{AMF} into a Linear Response Regime (LRR)[16] (Fig. 1 –top row). In this case, *M* uniquely shows hysteresis when $\tau_M \sim \tau_N$ due to a coupling over time between AMF and m_{NP}, describing characteristic ellipsoidal contours (Fig. 1 –top row). [17] Conversely, when $H_{AMF} > H_C$, m_{NP} overcome the magnetic anisotropy barrier $\Delta E=KV$, eventually collapsing into a fully saturated magnetization curve as long as H_{AMF} is strong enough. In this case, *M* versus H_{AMF} (*MvsH*) reflects a non-linear response regime (non-LRR) (see Fig. 1 –bottom row). Under these circumstances, *MvsH* loops will depict either a non-hysteretic, (i.e. unblocked or superparamagnetic state, SPM) or a hysteretic magnetic behaviour (i.e. blocked state, BS) depending on the τ_M / τ_N ratio (Fig. 1 –Bottom row).[17, 18] Several studies have proposed experimental techniques such as AC susceptometry[19, 20] to display transitions between magnetically unblocked/blocked states as an unequivocal fingerprint of superparamagnetism in magnetic suspensions. Even though these techniques cover an extensive f_{AMF} range and enable to analytically trace minor magnetization loops[16], the available H_{AMF} values are limited to few tens of kA/m at frequencies lower than 1 kHz, or to several tens of A/m in the MHz range. Beside, inductive AC magnetometry has also been employed for similar purposes, generating higher H_{AMF} up to hundreds of kA/m[21]. However, f_{AMF} is limited into a narrow range from few to several hundreds of kHz. [22-25] Despite the relevant insights provided by these techniques on probing the dynamical magnetic properties of nanoparticles,[19, 24] their limited extent of H_{AMF} and f_{AMF} values hinder to unequivocally display SPM/BS transitions at room temperature in most magnetic suspensions.

Magneto-optical based techniques offer alternative solutions to overcome the above-mentioned instrumental limitations. *Cuñado et al.* [26] recently reported the design a Kerr effect set-up for studying the magnetization process in non-transparent magnetic layers under distinct configurations, including dynamical conditions. The equivalent magneto-optical effect in optical transmission is the Faraday effect[27], which has been previously explored to perform magnetometry and susceptometry measurements in semi-transparent solid composites containing magnetic phases.[28-36] Magnetic field sensors based on Faraday effect have demonstrated GHz frequency responses with cut-off frequencies as high as 700 MHz for yttrium iron garnets[37]. Indeed, Verdet constant is independent from AMF conditions contrary to inductive magnetometry and susceptometry. Hence, dynamical field effects on magnetization cycles over an extensive range of f_{AMF} can be explored to track the evolution of magnetization cycles in magnetic suspensions.

Among magnetic nanoparticles, iron oxide nanoparticles (IONPs) have attracted an incommensurable interest among the nanomaterial community in recent decades.[38-43] New advances in colloidal chemistry allow nowadays the preparation of highly uniform size, shape and composition IONPs with tailored physic-chemical properties and high biocompatibility. The IONP magnetic properties are defined by the inverse spinel structure with oxygen forming a face-centered cubic crystal system[44]. In magnetite, all tetrahedral sites are occupied by Fe^{3+} and octahedral sites are occupied by both Fe^{3+} and Fe^{2+}. Maghemite differs from magnetite in that all or most of the iron is in the Fe^{3+} state and by the presence of cation vacancies in the octahedral sites. Due to the presence of Fe^{2+} and Fe^{3+} ions, IONPs show ferrimagnetic order[9] at room temperature. The outstanding control of the current IONP synthesis routes[4,5] benefits their use in emerging applications based on the opening of AC magnetization cycles under AMFs. Indeed, magnetic response of IONP suspensions under radio frequency AMF determines crucial parameters, such as magnetic losses, of high relevance in chemical catalysis, [45, 46] magnetic hyperthermia (MH)[47-50], or magnetization harmonics in magnetic particle imaging (MPI).[51, 52] Therefore, a better understanding of nanomagnetism at the non-LRR and at room temperature is mandatory to boost IONP emerging technologies.

Here, we report an experimental and theoretical study to demonstrate the transition from magnetically unblocked to blocked states at room temperature for magnetic suspensions of IONPs with distinct sizes (12 and 22 nm). We performed experimental magnetization measurements under AMF in a six-decades frequency range from 300 mHz to 138 kHz and field intensities up to 40 kA/m. Numerical simulations obtained through solving the stochastic Landau-Liftshitz-Gilbert (LLG) equations predict experimental observations. In addition, an empirical expression is proposed to determine K_{eff} from a blocking frequency (f_{block}) beyond which AC magnetization reflects non-reversible magnetization process. Our study sheds light on unequivocally determining the fingerprint of superparamagnetic behaviour of IONPs. At the same time, our results contribute to significantly improve the description of superparamagnetism in magnetic suspensions under dynamical conditions at room temperature.

Experimental

Iron oxide nanoparticles

Magnetic IONPs were synthesized by a thermal decomposition method of iron organic precursors in 1-octadecene described elsewhere.[53, 54] Then, IONP were transferred to aqueous media through ligand substitution with *meso*-2,3-dimercaptosuccinic acid. The studied IONPs are highly uniform in size and morphology, showing extremely good crystalline features. Consequently, magnetic losses of these highly crystalline and monodisperse IONP suspensions show excellent values.[54]

Size characterization

The size and shape of the studied IONPs were evaluated by transmission electron microscopy (TEM). JEOL JEM 2100 microscope operating at 100 kV was employed at Servicio Interdepartamental de Investigación, Universidad Autónoma de Madrid (Madrid, Spain). TEM images were examined through manual analysis of more than 150 particles randomly selected in different areas of TEM micrographs using Image-J software to obtain mean sizes and size distributions. TEM revealed average IONP core sizes of 12 ± 1 and 22 ± 2 nm (see Fig. S1) were reported elsewhere.[54]

Colloidal characterization

Colloidal characterization of selected IONPs was performed through hydrodynamic size (D_H) measurement by dynamic light scattering (DLS) in a Zetasizer Nano ZS equipment (Malvern Instruments, USA). In order to realize DLS measurements, IONPs were diluted in double distilled water (DDW) to a final concentration of 0.05 g_{Fe}/L in a commercial cuvette. The energy source was a laser emitting at 633 nm, and the angle between sample and detector was 173°.

Magnetic characterization

Quasi-static conditions: magnetic characterization of IONP (iron mass of 200 µg) under quasi-static conditions was carried out in a vibrating sample magnetometer (VSM, Oxford Instrument MLVSM9 MagLab 2-T). The variation of sample magnetization as a function of the with the applied external magnetic field was acquired at RT by first saturating the sample under a field of 1,6x10^{6}A/m. Magnetization units are expressed in Am^2/kg of the inorganic residue (magnetite and/or maghemite) as obtained by thermalgravimetric analysis. Zero field cooling/field cooling (ZFC/FC) measurements were performed in a temperature range from 5 to 260 K measuring magnetization while increasing *T* under a static magnetic field of H = 8 kA/m. Within this thermal range, IONP dispersions were frozen in order to perform precise magnetization measurements.

Dynamical conditions: AC Faraday effect-based magnetometer employed in this work uses a laser light to probe magnetic properties of iron oxide nanoparticles dispersed in DDW (see Fig. S2 at ESI). The magneto-optical set-up comprises the incident and transmitted beam's arms where all the optical and optomechanical components. In between, the sample holder is a glass tube surrounded by the AC magnetic field generation coil, and all electronics for driving and controlling the data acquisition. The laser light source is a non-polarised HeNe laser beam (632,8 nm, LHX1, Melles Griot and 0.1 W/cm^2 density power). The linear polarization of the incident light is selected by a linear polarizer located immediately after the laser output and in front of sample holder. A lens to collimate the laser beam into the photodetector, a λ/2 waveplate to align the polarized light with the Wollaston Prism axis and a dual in-house built photodetector to collect the orthogonal polarized beams generated in the Wollaston Prism (Fig. S2). In this set-up, AC magnetic fields were generated by an air-cooled Litz-wire coil whose gap holds a capillary glass tubes containing 20 microliters of IONP suspension in DDW. The coil was connected to a LCR circuit fed by an electronic signal generator TTi TG5011 whose signal is amplified by a home-made power amplifier. The AMF generator operates in a six decades frequency range from 300 mHz to 138 kHz, and field intensities up to 40 kA/m. To accurately determine H_C values, a synthetic quartz sample (2x2x1 mm) was employed as reference material. Experimental artifacts resulting in fake opening of magnetization cycles were removed by adjusting the magnetization signal of diamagnetic quartz at the tested AMF conditions (see Fig. S3).

Numerical simulations

Numerical simulations of AC magnetization loops were based on developing a theoretical model for $\vec{n}$ and $\vec{u}$, which are unit vectors along the easy axis and magnetic moment, respectively, based on numerically solving a modified version of the Landau-Liftshitz-Gilbert (LLG) equations:

$$\frac{d\vec{n}}{dt} = \frac{KV}{3\eta V_h}(\vec{u}\cdot\vec{n})[\vec{u} - (\vec{u}\cdot\vec{n})\vec{n}] + \sqrt{\frac{k_B T}{6\eta V_H}}\vec{\Gamma}\times\vec{n} \qquad (2)$$

$$\frac{d\vec{u}}{dt} = \mu_0\gamma\{\vec{u}\times(\vec{H}_{\text{eff}} + \vec{H}_{\text{th}}) - \lambda\vec{u}\times[\vec{u}\times(\vec{H}_{\text{eff}} + \vec{H}_{\text{th}})]\} \quad (3)$$

where μ_0 is the permeability of free space, η is the viscosity of the surrounding medium, V_h is the nanoparticle hydrodynamic volume, γ is the gyromagnetic ratio, λ is a dimensionless damping coefficient, $\vec{H}_{\text{eff}}$ is the effective magnetic field, $\vec{\Gamma}$ is the random torque, and $\vec{H}_{\text{th}}$ is the fluctuating magnetic field (more details in ESI).

Results and discussion

Magneto-optical Faraday effect experiments in magnetic suspensions under AMF at room temperature

We studied IONPs of 12 and 22 nm size with spherical and truncated octahedral shapes, respectively. These IONPs were dispersed in double distilled water (DDW) exhibiting hydrodynamic sizes (DH)/polydispersity indexes (PDI) of 49 nm/0.22 and 48 nm/0.17 for 12 and 22 nm size IONPs, respectively.[54] According to TEM images and DLS measurements, some degree of IONP aggregation was observed in both 12 and 22 nm IONP dispersions. In order to monitor the evolution of magnetization cycles under AMF at room temperature (298 K), we performed magneto-optical

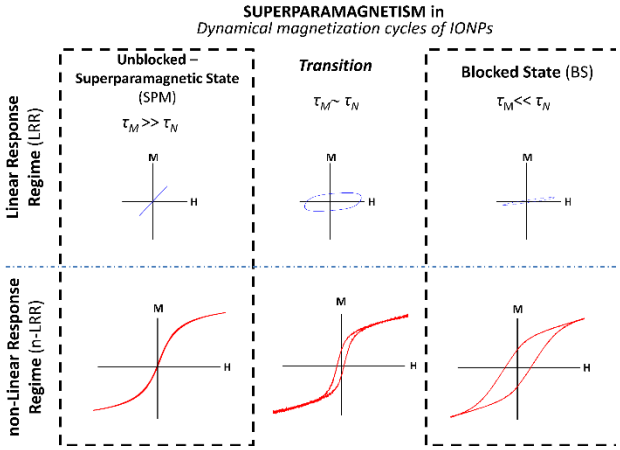

Fig. 1.- Schematic representation of magnetization loops of superparamagnetic nanoparticles observed at different dynamical conditions set by τ_m / τ_N ratios at LRR and non-LRR.

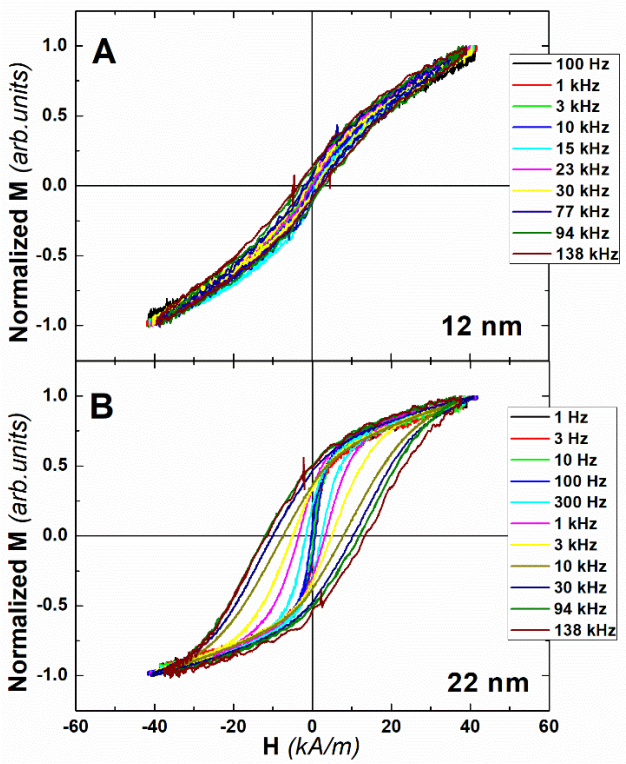

Fig. 2.- Frequency dependence of normalized AC magnetization cycles of magnetic suspensions at room temperature (298 K) for A) 12nm IONPs; B) 22nm IONPs. Nanoparticles were dispersed in DDW at [Fe]=0.4g/L.

measurements in a home-made magnetometer based on Faraday effect[55] (see Experimental Section). This set-up allows to acquire magnetisation loops of magnetic DDW suspensions in a six decades f_{AMF} range from 300 mHz up to 138 kHz and H_{AMF} up to 40 kA/m. The IONP concentration values of the studied magnetic suspensions $\leq 0.4 g_{Fe}/L$ to maximize the light transmission signal. The highly diluted IONP dispersions warrant no influence of inter-aggregate magnetic dipolar interactions on their dynamical magnetic properties.[56] Fig. 2 shows the frequency dependence of AC magnetisation cycles of the studied IONP dispersions. The evolution of *MvsH* loops with frequency reflect the appearance of the opening of AC magnetization loops. Hysteretic magnetization cycles appear at different frequency values depending on IONP size, although common features are observed. At low f_{AMF} (<20 Hz), *MvsH is* characterised by reversible magnetization cycles with no traces of hysteretic behaviour (i.e. M_R and $H_C = 0$), typical from SPM state. At high f_{AMF} (> 20 Hz) non-reversible magnetization cycles (M_R and $H_C > 0$) are observed in magnetization cycles i.e., hysteretic behaviour characteristic from BS states. For a better display of SPM/BS transitions for both IONPs, the frequency dependence of coercive field (H_C) of these magnetisation loops was determined for its representation as a function of f_{AMF}. As shown in Fig. 3, both IONPs show $H_C = 0$ at f_{AMF} values $\leq$ 20 Hz. However, H_C differently evolves at higher frequencies depending on IONP size. While 22nm IONPs shows a progressive increase of H_C beyond 20 Hz, 12nm IONP maintains zero coercivity up to 13 kHz. Beyond this frequency, H_C begins to progressively increase up to the final f_{AMF} (138 kHz) where H_C = 4,2 kA/m for 12nm IONPs. The latest is nearly four times smaller than the value obtained for the 22nm ones at the same f_{AMF} (H_C=15,6 kA/m). Such distinct H_C values are consequently reflected in magnetic area and related magnetic losses. Indeed, previous report[54] shows that the Specific Absorption Rate (*SAR*) of the studied IONPs are significantly higher for 22nm IONPs (*SAR*= 323 W/g_{Fe}) than for 12nm (*SAR*= 14 W/g_{Fe}) at 77 kHz and 40 kA/m. Note that the transition from reversible (SPM) to non-reversible (BS) magnetization processes occurs at very different f_{AMF} values depending on IONP size: 13 kHz for 12nm IONPs and 20 Hz for 22nm IONPs. This transition from SPM to BS states can be understood in terms of the IONP magnetic dynamics (i.e. magnetic relaxation). When $\tau_N < \tau_M$, magnetization loops are fully reversible because thermally mediated relaxation processes of m_{NP} are quicker than the measurement time, preventing the appearance of AC magnetic hysteresis.[57, 58] Contrary, when $\tau_N > \tau_M$ *MvsH* loops are characterised by non-reversible magnetization processes depicting hysteretic behaviour (see Fig. 2). Under these conditions, magnetic moments of nanoparticles are directionally blocked by the magnetic anisotropy of the crystals, and solely reversed by the external AMF action.[59]

Numerical simulations of frequency dependence of AC magnetisation loops

In order to theoretically describe our experimental findings, numerical simulations based on the stochastic LLG equations were performed to model magnetization cycles along the studied frequency range (see Experimental Section). This model has been previously employed for successfully describing viscosity effects on AC hysteresis loops at 100 kHz at LLR and non-LRR[24]. Our theoretical model includes the following assumptions: i) interacting nanoparticles are not considered; ii) coexistence of Brownian and Néel magnetic relaxation processes; iii) particle size distribution is neglected. As reflected in the good agreement with experiments shown in Fig. 3, such assumptions do not represent strong limitations. It is worth noting that the studied IONPs are highly crystalline and have narrow size distribution, and homogenous shape.[53,54] Furthermore, previous results[54] from calorimetry and magnetometry experiments performed in the studied IONPs shows that Néel relaxation process prevails. However, Brownian mechanism [60] is included since IONPs are suspended in liquids. Consequently, Brownian relaxation process can also contribute to reorientate the m_{NP} direction, competing against Néel one. Generally, it is well accepted that both Néel and Brownian relaxation mechanisms coexist and contribute into an effective relaxation time (τ_{eff}) given by the expression $1/\tau_{eff} = 1/\tau_N + 1/\tau_B$, where $\tau_B = 3\eta V_H/k_B T$ is Brownian relaxation time. However, it is worth to note that the internal and spontaneous m_{NP} reorientation dynamics is described by Eq.1, involves only Néel process. Therefore, Brownian relaxation may be considered as an extrinsic relaxation process for magnetic nanoparticles. Numerical simulations shown in Fig.3 depicted an excellent agreement

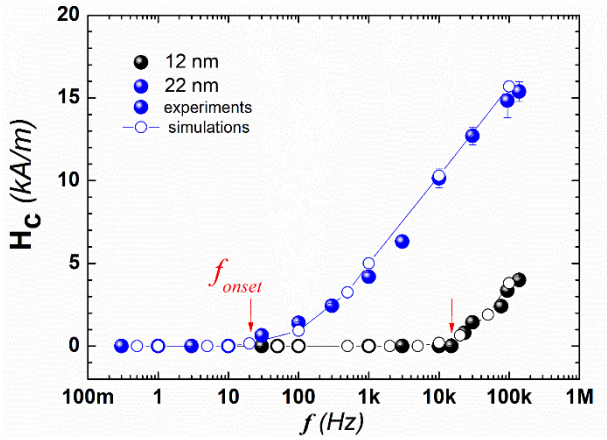

Fig. 3.- Experimental (filled dots) and theoretical (empty dots) frequency dependence of coercive field (H_C) for 12nm (black dots) and 22nm (blue dots) IONPs (H_{AMF}= 40 kA/m) extracted from Figure 2. Red arrows indicate the blocking frequencies (f_{block}).

between experimental (solid dots) and simulated (empty dots) for describing the frequency dependence of HC along the studied frequency range for both IONP sizes (22nm blue and 12nm black colours).

In general terms, a reasonable fit was also found between the experimental and simulated *MvsH* loops (Fig. S4), although some disparities are found mainly in the non-lineal region of magnetization curves.[61] These discrepancies may be attributed to the intra-aggregate magnetic dipolar interactions between nanoparticles,[56] which were not explicitly considered in our calculations, as well as a dissimilar orientation of the easy axis of the IONPs between the experimental and theoretical data. Anyhow, numerical simulations accurately predict the evolution of H_C in the broad frequency range shown in Fig.3.

Determination of magnetic anisotropy from blocking frequency values

Magnetic anisotropy K_{eff} is generally determined in FC-ZFC measurements by stablishing a blocking temperature T_B.[62, 63] Negligible Brownian relaxation contribution in the studied IONPs enable to stablish a new method to calculate K_{eff} by defining an empirical expression for f_{block}:

$$f_{block} = \frac{f_N}{100} = \frac{1}{100 \cdot 2\pi \tau_N} \qquad (4)$$

Since σ (defined in eq. 1) cannot be analytically derived from eq. 4, we performed numerical simulations (see Fig. S6 at ESI) to obtain the following expression to correlate K_{eff} through f_{block}:

$$K_{\text{eff}} = \frac{k_B T}{V} [-2.4064 \times \log(f_{block}) + 15.745] \qquad (5)$$

where $V = \pi\, d_C{}^3 / 6$ is the IONP volume, and d_C is the IONP size. Thus, we obtain the K_{eff} values of 26 kJ/m^3 for 12nm IONPs and 9.2 kJ/m^3 for 22nm IONPs. One of the advantages of the employed technique to determine K_{eff} compared with others based on ZFC/FC[54] or H_c[64] measurements is that K_{eff} can be determined from the f_{block} value at room temperatures. Thus, Faraday magnetometry offers an alternative technique to determine K_{eff} based on the f_{block} beyond which SPM/BS transition occurs at non-LRR.

In order to assess the validity of our method, we performed quasi-static magnetization and ZFC/FC measurements by VSM for probing the transition from BS to SPM states and determining K_{eff} from T_B. As shown in Fig. S5, VSM magnetisation measurements at low temperatures show hysteretic cycles for the studied IONPs with distinct H_C values (H_C =20 kA/m and 27 kA/m for 12 and 22nm, respectively). At low temperatures, most of the magnetic moments are thermally blocked for both IONPs, disabling any possible thermally-ruled relaxation mechanisms (i.e. $\tau_N \rightarrow \infty$; Eq. 1). However, such hysteretic behaviour observed in VSM measurements (Fig. S5) smears out near room temperatures. While VSM magnetisation loops for 12nm IONP reflects a SPM behaviour at 250 K (i.e. H_C=0), 22nm IONPs still maintains a BS behaviour (i.e. H_C=1,5 kA/m). In order to test the validity of K_{eff} value obtained by Eq.5, we simulated the quasi-static VSM magnetisation loops at 250 K with our LLG model. As shown in Fig.4, the agreement with experiments is good when using the effective anisotropy values like those obtained through Eq. 4 (K_{eff}=26 kJ/m^3 for 12nm and 9.5 kJ/m^3 for 22nm IONPs core size vs 26 and 9.2 kJ/m^3 obtained by the empirical expression). In particular, the agreement between VSM experimental and simulated magnetization is excellent for 12 nm IONPs. However, for the case of 22nm IONPs, simulation fails to precisely predict the saturation magnetization value and magnetization field dependence beyond the linear response region (Fig. 4B). We speculate that the disagreement between experiments and theory is related to intra-aggregate magnetic dipolar interactions, which are not included in the simulations and have been shown to become relevant for 22 nm IONPs.[54] Nevertheless, the prediction of the magnetization at the linear response range (< 80 kA/m) accurately matches experimental results, allowing to predict the evolution of H_C in the broad frequency range as shown in Fig.3.

To further validate our empirical expression, we compared K_{eff} values obtained through Eq. 4 with those derived from ZFC/FC measurements (Figs. S5 B,D). Thus, by determining the blocking temperature T_B, we extracted the effective magnetic anisotropy values ($\Delta E = KV$). We determined T_B = 140 K for 12nm and 270 K for 22nm IONPs. Assuming spherical volumes, we obtained K_{eff} =5.3 x 10^4 J/m^3 and 1.8 x 10^4 J/m^3, respectively, finding a reasonable consonance in terms of order of magnitude the ZFC/FC and Eq. 6 derived values. Regarding this difference between ZFC/FC values, note that the precision determining T_B tightly depends on how abrupt the BS/SPM transition arises in FC/ZFC curves.[63,65] Indeed, a significant margin of uncertainty on the experimental K_{eff} values can be assumable in slightly polydisperse and interacting magnetic suspensions. [63, 65] This could explain the differences in K_{eff} values found between the empirical expression (Eq. 6) and the ZFC/FC measurements. In addition to this, it is important to remark that the empirical expressions Eq. 4 and 5 has been applied only for IONPs with narrow size distribution.[53,54] IONPs with larger distribution, the

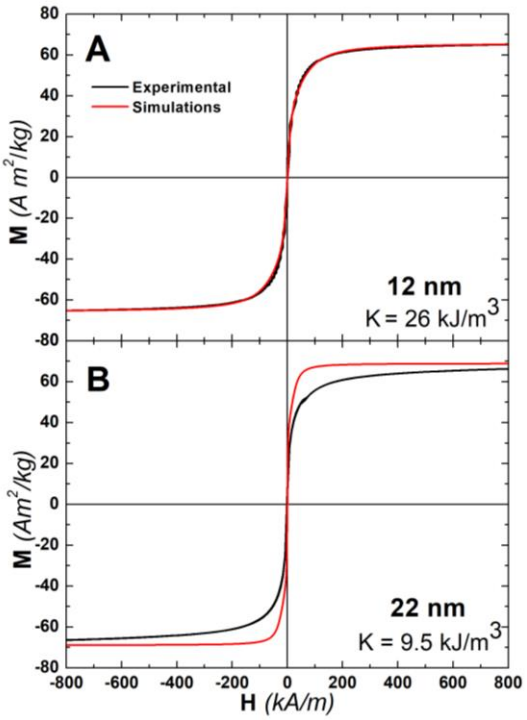

Fig. 4.- Comparison between VSM measurement (red colour) and simulated (blue colour) magnetization cycles under quasi-static conditions for A) 12 and B) 22 nm size IONPs dispersed in DDW at $2g_{Fe}$ /L and 250 K.

largest value of nanoparticle volume V should be utilised, as those have the biggest potential to delimitate the f_{block}.

Conclusions

We have experimentally demonstrated the room temperature transition from non-hysteretic to hysteretic behaviour of magnetization cycles measured in IONP suspensions subjected to AMF in the non-LRR. We have used an AC Faraday effect-based magnetometry set-up working in an extremely broad field frequency range from mHz to hundreds of kHz with field intensities up to 40 kA/m. Experimental results exhibited a room temperature transition from superparamagnetic (unblocked) to blocked states, associated with Néel relaxation processes of IONP magnetic moments, while subjected to AMF in the non-LRR. This transition occurs at field frequency values which depends on IONP size. Consequently, larger opening of AC magnetization loops is observed for larger IONPs in the studied filed condition range. Theoretical calculations based on providing numerical solutions to the stochastic LLG equations allows to describe the experimental observations in terms of the distinct magnitude of magnetic anisotropy barrier of the studied IONP suspensions. The good aggreement between theory and experiment yields to an empirical expression to determine K_{eff} from the f_{block} value beyond which AC magnetization becomes hysteretic under non-LRR. Our results unveil an unambiguous fingerprint of SPM-BS transition in magnetic suspensions related to superparamagnetic behaviour. New numerical tools are provided for predicting interesting magnetic phenomena related to IONPs and of high interest in catalysis and biomedical applications.

Author contributions

JC and FJT designed the research. GS and MPM prepared and characterised the studied IONP. JC, AB, JLFC and FJT set up the magneto-optical Faraday magnetometer. TRD, AB, JLFC and FJT performed magneto-optical experiments. DC, TRD, FJT and JC analysed and discussed the results. TY performed the numerical simulations and discussed the results with DC and FJT. DC and FJT wrote the first draft, and the rest of authors contribute to tail the submitted and revised manuscripts.

Conflicts of interest

There are no conflicts to declare.

Acknowledgements

This work has been partially funded by Spanish Ministry of Science, Innovation and Universities (PCI2019-103600, RYC2011- 09617, SEV-2016-0686,) and Comunidad de Madrid (NANOMAGCOST, S2018/NMT-4321). Spanish Scientific Network (Hipernano, RED2018-102626-T), European COST Actions CA17115 (MyWave), and CA17140 (Nano2Clinic) are also acknowledged. Authors thank Dr. Hector Guerrero for the rigorous reading and constructive comments on this manuscript.

References

1. W. Lei, J. Xu, Y. Yu, W. Yang, Y. Hou and D. Chen, *Nano Letters*, 2018, **18**, 7839-7844.
2. K. Sartori, F. Choueikani, A. Gloter, S. Begin-Colin, D. Taverna and B. P. Pichon, *Journal of the American Chemical Society*, 2019, **141**, 9783-9787.
3. X. Liu, Y. Tian and L. Jiang, *Nano Letters*, 2021, **21**, 2699-2708.
4. A. G. Roca, L. Gutiérrez, H. Gavilán, M. E. Fortes Brollo, S. Veintemillas-Verdaguer and M. d. P. Morales, *Advanced Drug Delivery Reviews*, 2019, **138**, 68-104.
5. H. Gavilán, S. K. Avugadda, T. Fernández-Cabada, N. Soni, M. Cassani, B. T. Mai, R. Chantrell and T. Pellegrino, *Chemical Society Reviews*, 2021, **50**, 11614-11667.
6. K. M. Krishnan, *Fundamentals and Applications of Magnetic Materials*, Oxford University Press, Oxford, 2016.
7. L. Néel, *Proceedings of the Physical Society. Section A*, 1952, **65**, 869-885.
8. M. L. Néel, *Ann. Phys.*, 1948, **12**, 137-198.
9. B. D. Cullity and C. D. Graham, in *Introduction to Magnetic Materials*, 2008, DOI: https://doi.org/10.1002/9780470386323.ch6, pp. 175-195.
10. B. D. Cullity, Graham, C.D. , in *Introduction to Magnetic Materials*, 2008, DOI:

https://doi.org/10.1002/9780470386323.ch4, pp. 115-149.
11. C. P. Bean and J. D. Livingston, *Journal of Applied Physics*, 1959, **30**, S120-S129.
12. P. M. Enriquez-Navas and M. L. Garcia-Martin, in *Frontiers of Nanoscience*, eds. J. M. de la Fuente and V. Grazu, Elsevier, 2012, vol. 4, pp. 233-245.
13. W. F. Brown, *Physical Review*, 1963, **130**, 1677-1686.
14. C. N. Scully, P. J. Cregg and D. S. F. Crothers, *Physical Review B*, 1992, **45**, 474-476.
15. L. Néel, *J. Phys. Radium*, 1950, **11**, 49-61.
16. R. E. Rosensweig, *Journal of Magnetism and Magnetic Materials*, 2002, **252**, 370-374.
17. N. Telling, in *Nanomaterials for Magnetic and Optical Hyperthermia Applications*, eds. R. M. Fratila and J. M. De La Fuente, Elsevier, 2019, DOI: https://doi.org/10.1016/B978-0-12-813928-8.00007-7, pp. 173-197.
18. J. Wallyn, N. Anton and T. F. Vandamme, *Pharmaceutics*, 2019, **11**, 601.
19. D. Cabrera, A. Coene, J. Leliaert, E. J. Artés-Ibáñez, L. Dupré, N. D. Telling and F. J. Teran, *ACS Nano*, 2018, **12**, 2741-2752.
20. F. Ahrentorp, A. P. Astalan, C. Jonasson, J. Blomgren, B. Qi, O. T. Mefford, M. Yan, J. Courtois, J. F. Berret, J. Fresnais, O. Sandre, S. Dutz, R. Müller and C. Johansson, *AIP Conference Proceedings*, 2010, **1311**, 213-223.
21. I. Rodrigo, I. Castellanos-Rubio, E. Garaio, O. K. Arriortua, M. Insausti, I. Orue, J. Á. García and F. Plazaola, *International Journal of Hyperthermia*, 2020, **37**, 976-991.
22. V. Connord, B. Mehdaoui, R. P. Tan, J. Carrey and M. Respaud, *Review of Scientific Instruments*, 2014, **85**, 093904-093904.
23. E. Garaio, J. M. Collantes, J. A. Garcia, F. Plazaola, S. Mornet, F. Couillaud and O. Sandre, *Journal of Magnetism and Magnetic Materials*, 2014, **368**, 432-437.
24. D. Cabrera, A. Lak, T. Yoshida, M. E. Materia, D. Ortega, F. Ludwig, P. Guardia, A. Sathya, T. Pellegrino and F. J. Teran, *Nanoscale*, 2017, **9**, 5094-5101.
25. D. Cabrera, I. Rubia-Rodríguez, E. Garaio, F. Plazaola, L. Dupré, N. Farrow, F. J. Terán and D. Ortega, in *Nanomaterials for Magnetic and Optical Hyperthermia Applications*, eds. R. M. Fratila and J. M. De La Fuente, Elsevier, 2019, DOI: https://doi.org/10.1016/B978-0-12-813928-8.00005-3, pp. 111-138.
26. J. L. F. Cuñado, A. Bollero, T. Pérez-Castañeda, P. Perna, F. Ajejas, J. Pedrosa, A. Gudín, A. Maldonado, M. A. Niño, R. Guerrero, D. Cabrera, F. J. Terán, R. Miranda and J. Camarero, *Scientific Reports*, 2017, **7**, 13474.
27. P. Day, *The Philosopher's Tree: A Selection of Michael Faraday's Writings*, CRC Press, New York, 1st edn., 1999.
28. E. Taboada, R. P. del Real, M. Gich, A. Roig and E. Molins, *Journal of Magnetism and Magnetic Materials*, 2006, **301**, 175-180.
29. J. L. Menendez, L. Fernandez-Garcia, C. Pecharroman, I. Montero, A. Esteban-Cubillo, P. Tiemblo and N. Garcia, *Opt. Mater. Express*, 2015, **5**, 1927-1933.
30. N. G. Pavlopoulos, K. S. Kang, L. N. Holmen, N. P. Lyons, F. Akhoundi, K. J. Carothers, S. L. Jenkins, T. Lee, T. M. Kochenderfer, A. Phan, D. Phan, M. E. Mackay, I. B. Shim, K. Char, N. Peyghambarian, L. J. LaComb, R. A. Norwood and J. Pyun, *Journal of Materials Chemistry C*, 2020, **8**, 5417-5425.
31. S. Kucukdermenci, D. Kutluay and I. Avgin, *Mater. Tehnol.*, 2013, **47**, 71-78.
32. K. S. Buchanan, A. Krichevsky, M. R. Freeman and A. Meldrum, *Physical Review B*, 2004, **70**, 174436.
33. R. P. del Real, G. Rosa and H. Guerrero, *Review of Scientific Instruments*, 2004, **75**, 2351-2355.
34. H. Guerrero, G. Rosa, M. P. Morales, F. del Monte, E. M. Moreno, D. Levy, R. Pérez del Real, T. Belenguer and C. J. Serna, *Applied Physics Letters*, 1997, **71**, 2698-2700.
35. P. K. Jain, Y. Xiao, R. Walsworth and A. E. Cohen, *Nano Letters*, 2009, **9**, 1644-1650.
36. M. Domínguez, D. Ortega, J. S. Garitaonandía, R. Litrán, C. Barrera-Solano, E. Blanco and M. Ramírez-del-Solar, *Journal of Magnetism and Magnetic Materials*, 2008, **320**, e725-e729.
37. M. Deeter, K. B. Rochford, A. Rose and G. W. Day, 1993.
38. T. Vangijzegem, D. Stanicki and S. Laurent, *Expert Opinion on Drug Delivery*, 2019, **16**, 69-78.
39. S. S. Leong, S. P. Yeap and J. Lim, *Interface Focus*, 2016, **6**, 20160048.
40. I. K. Herrmann, A. A. Schlegel, R. Graf, W. J. Stark and B. Beck-Schimmer, *Journal of nanobiotechnology*, 2015, **13**, 49-49.
41. D. Cabrera, K. Walker, S. Moise, N. D. Telling and A. G. S. Harper, *Nano Research*, 2020, **13**, 2697-2705.
42. T. A. P. Rocha-Santos, *TrAC Trends in Analytical Chemistry*, 2014, **62**, 28-36.
43. M. Mahmoudi, M. A. Sahraian, M. A. Shokrgozar and S. Laurent, *ACS chemical neuroscience*, 2011, **2**, 118-140.
44. R. M. Cornell and U. Schwertmann, in *The Iron Oxides*, 2003, DOI: https://doi.org/10.1002/3527602097.ch2, pp. 9-38.
45. Z. J. Díaz-Puerto, Á. Raya-Barón, P. W. N. M. van Leeuwen, J. M. Asensio and B. Chaudret, *Nanoscale*, 2021, **13**, 12438-12442.
46. Q. Zhang, X. Yang and J. Guan, *ACS Applied Nano Materials*, 2019, **2**, 4681-4697.
47. D. Ortega and Q. A. Pankhurst, in *Nanoscience: Volume 1: Nanostructures through Chemistry*, The Royal Society of Chemistry, 2013, vol. 1, pp. 60-88.
48. E. A. Périgo, G. Hemery, O. Sandre, D. Ortega, E. Garaio, F. Plazaola and F. J. Teran, *Applied Physics Reviews*, 2015, **2**, 041302.
49. D. Chang, M. Lim, J. A. C. M. Goos, R. Qiao, Y. Y. Ng, F. M. Mansfeld, M. Jackson, T. P. Davis and M. Kavallaris, *Frontiers in Pharmacology*, 2018, **9**.
50. I. Rubia-Rodríguez, A. Santana-Otero, S. Spassov, E. Tombácz, C. Johansson, P. De La Presa, F. J. Teran, M. d. P. Morales, S. Veintemillas-Verdaguer, N. T. K. Thanh, M. O. Besenhard, C. Wilhelm, F. Gazeau, Q. Harmer, E. Mayes, B. B. Manshian, S. J. Soenen, Y. Gu, Á. Millán, E. K. Efthimiadou, J. Gaudet, P. Goodwill, J. Mansfield, U. Steinhoff, J. Wells, F. Wiekhorst and D. Ortega, *Materials*, 2021, **14**, 706.
51. L. C. Wu, Y. Zhang, G. Steinberg, H. Qu, S. Huang, M. Cheng, T. Bliss, F. Du, J. Rao, G. Song, L. Pisani, T. Doyle, S. Conolly, K. Krishnan, G. Grant and M. Wintermark, *AJNR Am J Neuroradiol*, 2019, **40**, 206-212.
52. B. Gleich and J. Weizenecker, *Nature*, 2005, **435**, 1214-1217.

53. G. Salas, C. Casado, F. J. Teran, R. Miranda, C. J. Serna and M. P. Morales, *Journal of Materials Chemistry*, 2012, **22**, 21065-21075.
54. G. Salas, J. Camarero, D. Cabrera, H. Takacs, M. Varela, R. Ludwig, H. Dähring, I. Hilger, R. Miranda, M. d. P. Morales and F. J. Teran, *The Journal of Physical Chemistry C*, 2014, **118**, 19985-19994.
55. Rayleigh, *Nature*, 1901, **64**, 577-578.
56. J. G. Ovejero, D. Cabrera, J. Carrey, T. Valdivielso, G. Salas and F. J. Teran, *Physical Chemistry Chemical Physics*, 2016, **18**, 10954-10963.
57. D. D. Majumder, D. D. Majumder and S. Karan, in *Ceramic Nanocomposites*, eds. R. Banerjee and I. Manna, Woodhead Publishing, 2013, DOI: https://doi.org/10.1533/9780857093493.1.51, pp. 51-91.
58. W. R. L. Lambrecht, in *Rare Earth and Transition Metal Doping of Semiconductor Materials*, eds. V. Dierolf, I. T. Ferguson and J. M. Zavada, Woodhead Publishing, 2016, DOI: https://doi.org/10.1016/B978-0-08-100041-0.00002-0, pp. 43-101.
59. B. Martínez, F. Sandiumenge, L. Balcells, J. Arbiol, F. Sibieude and C. Monty, *Physical Review B*, 2005, **72**, 165202.
60. P. J. W. Debye, *Polar molecules*, The Chemical Catalog Company, Inc., New York, 1929.
61. M. Respaud, *Journal of Applied Physics*, 1999, **86**, 556-561.
62. G. Concas, F. Congiu, G. Muscas and D. Peddis, *The Journal of Physical Chemistry C*, 2017, **121**, 16541-16548.
63. K. L. Livesey, S. Ruta, N. R. Anderson, D. Baldomir, R. W. Chantrell and D. Serantes, *Scientific Reports*, 2018, **8**, 11166.
64. K. Enpuku, S. Draack, F. Ludwig and T. Yoshida, *Journal of Applied Physics*, 2021, **130**, 183901.
65. I. J. Bruvera, P. M. Zélis, M. P. Calatayud, G. F. Goya and F. H. Sánchez, *Journal of Applied Physics*, 2015, **118**, 184304.